



CHALMERS
UNIVERSITY OF TECHNOLOGY

Adipose-Derived Stromal Cells Preserve Pancreatic Islet Function in a Transplantable 3D Bioprinted Scaffold

Downloaded from: <https://research.chalmers.se>, 2024-05-04 01:51 UTC

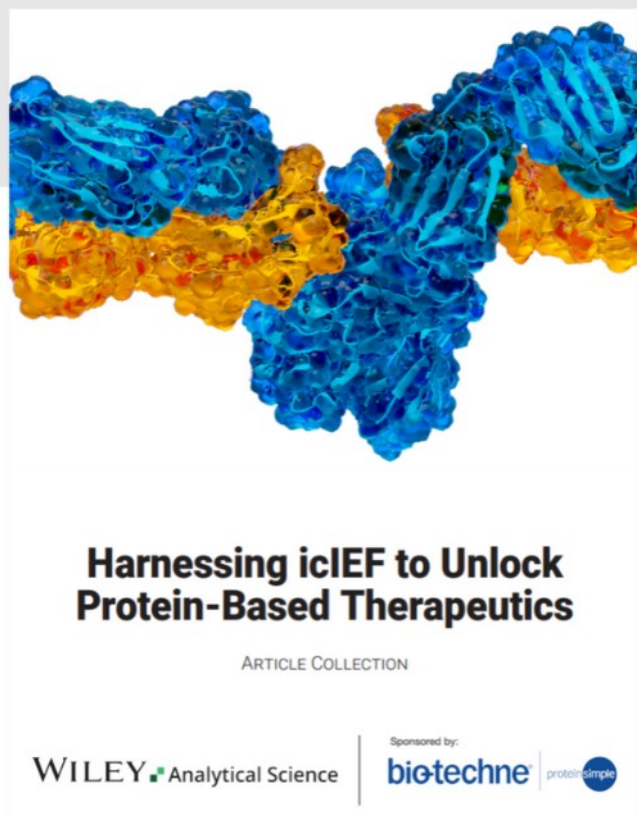
Citation for the original published paper (version of record):

Abadpour, S., Niemi, E., Strid Orrhult, L. et al (2023). Adipose-Derived Stromal Cells Preserve Pancreatic Islet Function in a Transplantable 3D Bioprinted Scaffold. *Advanced healthcare materials*, 12(32).
<http://dx.doi.org/10.1002/adhm.202300640>

N.B. When citing this work, cite the original published paper.



Harnessing icIEF to Unlock Protein-Based Therapeutics



Read the new Article Collection

Keep up to date with the latest developments in biotherapeutics and the range of treatments for various diseases with our latest article collection. Find out how imaged cIEF (icIEF) technique is essential for quality control and analytical development of these drugs, as it accurately determines the surface charge of lipid nanoparticles and the charge heterogeneity of proteins and antibodies.

This article collection aims to provide you with more information on these techniques and technologies, helping you further your research in this field.

Adipose-Derived Stromal Cells Preserve Pancreatic Islet Function in a Transplantable 3D Bioprinted Scaffold

Shadab Abadpour,* Essi M. Niemi, Linnea Strid Orrhult, Carolin Hermanns, Rick de Vries, Liebert Parreiras Nogueira, Håvard Jostein Haugen, Dag Josefsen, Stefan Krauss, Paul Gatenholm, Aart van Apeldoorn, and Hanne Scholz*


Intra-portal islet transplantation is currently the only clinically approved beta cell replacement therapy, but its outcome is hindered by limited cell survival due to a multifactorial reaction against the allogeneic tissue in liver. Adipose-derived stromal cells (ASCs) can potentially improve the islet micro-environment by their immunomodulatory action. The challenge is to combine both islets and ASCs in a relatively easy and consistent long-term manner in a deliverable scaffold. Manufacturing the 3D bioprinted double-layered scaffolds with primary islets and ASCs using a mix of alginate/nanofibrillated cellulose (NFC) bioink is reported. The diffusion properties of the bioink and the supportive effect of human ASCs on islet viability, glucose sensing, insulin secretion, and reducing the secretion of pro-inflammatory cytokines are demonstrated. Diabetic mice transplanted with islet-ASC scaffolds reach normoglycemia seven days post-transplantation with no significant difference between this group and the group received islets under the kidney capsules. In addition, animals transplanted with islet-ASC scaffolds stay normoglycemic and show elevated levels of C-peptide compared to mice transplanted with islet-only scaffolds. The data present a functional 3D bioprinted scaffold for islets and ASCs transplanted to the extrahepatic site and suggest a possible role of ASCs on improving the islet micro-environment.

1. Introduction

Beta cell replacement therapy with the help of scaffolds delivering cells give a possibility to radically change the treatment of type 1 diabetes (T1D) by improving the efficacy, accessibility, and safety of transplantation of insulin-producing islet cells. Currently, clinical islet transplantation (CIT) via the hepatic portal vein is the standard method utilized in clinical settings. This approach has demonstrated a significant enhancement in glycemic control and effectively eliminating the requirement for insulin therapy in patients with severe T1D for several years.^[1,2] However, CIT is limited by several confounding factors that lead to a loss of $\approx 50\%$ of the transplant in the first weeks after transplantation.^[3,4] These factors include inadequate vascularization, poor engraftment, immediate blood mediated inflammatory reaction, long-term allo- and auto-immunity, high concentrations of lipids and glucose, and immunosuppressive drugs that are present in the hepatic vasculature. All these factors cause

S. Abadpour, H. Scholz
Department of Transplant Medicine
Oslo University Hospital
Oslo 0372, Norway
E-mail: shadab.abadpour@medisin.uio.no;
hanne.scholz@medisin.uio.no
S. Abadpour, E. M. Niemi, H. Scholz
Institute for Surgical Research
Oslo University Hospital
Oslo 0372, Norway

S. Abadpour, E. M. Niemi, S. Krauss, H. Scholz
Hybrid Technology Hub – Centre of Excellence
Institute of Basic Medical Sciences
University of Oslo
Oslo 0372, Norway
E. M. Niemi
Department of Vascular Surgery
Aker Hospital
Oslo University Hospital
Oslo 0586, Norway
L. S. Orrhult, P. Gatenholm
3D Bioprinting Center
WWSC
Department of Chemistry and Chemical Engineering
Chalmers University of Technology
Gothenburg 41296, Sweden
C. Hermanns, R. de Vries, A. van Apeldoorn
MERLN Institute for Technology-Inspired Regenerative Medicine
Maastricht University
Maastricht 6229, The Netherlands

 The ORCID identification number(s) for the author(s) of this article can be found under <https://doi.org/10.1002/adhm.202300640>

© 2023 The Authors. Advanced Healthcare Materials published by Wiley-VCH GmbH. This is an open access article under the terms of the Creative Commons Attribution-NonCommercial License, which permits use, distribution and reproduction in any medium, provided the original work is properly cited and is not used for commercial purposes.

DOI: 10.1002/adhm.202300640

loss of islets, leading to multiple CIT procedures to reach insulin independence without any guarantee for long-term survival of the transplanted islet grafts.^[5–7] Delivery of islets in hydrogel-based scaffolds have been explored over the years in several diabetic in vivo models and reported to have partial islet function and protection from immune rejection.^[8] However, using large scaffolds comes with a price of limited oxygen, nutrients and insulin transports to and from the encapsulated islets, which subsequently lead to decreased islet survival and function.^[9–12]

Three-dimensional (3D) bioprinting could provide the advantages of a macroscopic delivery approach by retaining multiple islets in one potentially flat scaffold. This could offer a short diffusion distance to the surface which is an advantage for nutrient exchange and glucose sensing. 3D bioprinting could also provide an internal mesh-like porous structure to keep the islets in place between the hydrogel fibrils. By creating a porous 3D bioprinted scaffolds which allow the ingrowth of vasculature around and in, one single delivery scaffold could be transplanted to any extrahepatic site of choice.^[13–15] 3D bioprinting is explored for cell delivery applications as it allows for the creation of a pre-designed scaffold architecture using computer-aided design.^[16–21] It provides relatively good control over homologous cell distribution within a scaffold, and it gives a possibility to use multiple cell types in a fabricated 3D cell scaffold.^[22] Alginate has been explored as a biomaterial in the field of islet encapsulation for over two decades and also recently in 3D bioprinting applications because of its high biocompatibility and low cytotoxicity.^[23] Despite robustness of alginate in generating islet microcapsules, the favorable concentration of 1.5% for islet encapsulation complicates 3D bioprinting. In addition, the low viscosity of the uncrosslinked alginate prevents shape retention during the fibril dispositioning.^[24] Cellulose is a natural biopolymer and has been suggested as a potential biomaterial with suitable shear thinning properties and good biocompatibility.^[25] Nanofibrillated cellulose (NFC) is cellulose fibers that have been fibrillated in order to achieve agglomerates of cellulose microfibril units with the size of normally less than 100 nm in diameter and the length of several micrometers.^[26] A mixture of alginate/NFC has been investigated to create 3D bioprinted scaffolds that are stable in shape for example in cartilage related, human ear pinna and sheep meniscus applications.^[27–30] Only recently, alginate-based 3D bioprinting has been applied for pancreatic islets and stem cell-derived insulin-producing cells.^[31,32]

Marchioli et al. demonstrated the proof-of-principle for bioprinting primary islets with alginate and alginate-gelatin mixture.^[33] Likewise, Duin et al. 3D bioprinted pancreatic islet scaffolds by using alginate-methylcellulose bioink.^[32] However, islets in these 3D bioprinting scaffolds reported poor functionality in regards to glucose sensing and insulin secretion likely due to the hydrogel composition that prevented proper insulin secretion from the resulting scaffolds.^[32,33] Bioprinting of islets with biomaterials, like other cell encapsulation methods create a barrier for diffusion of nutrients, oxygen and insulin to and from the islets, which might cause delay or hinder glucose sensing and insulin secretion.^[34] During the islet isolation procedure, islets get exposed to radical changes in their micro-environment due to a combination of enzymatic digestion and mechanical disruption of pancreatic tissue.^[35,36] These changes induce stress-related cell signaling to islets which can lead to diminished cell survival and loss of islet function. Combination of these factors potentially reduce the function and viability of 3D bioprinted islet scaffolds.^[8,31,32] Interestingly, Marchioli et al. showed that the 3D bioprinting process itself did not harm the islets and they suggest that a more optimal hydrogel composition is needed for 3D bioprinting with proper mass transport capabilities to support beta cell function. Potentially, mixing hydrogel-based bioink with extracellular matrix (ECM) molecules obtained from pancreatic tissue is one strategy to improve islet health post-printing.^[37] A recent published study demonstrated the use of porcine ECM from decellularized pancreas in hydrogel-based bioink improved islet health and induced angiogenesis 90 days post-transplantation in a diabetic mouse model.^[38] However, implication of such strategy on clinical islet transplantation could add extra challenges including the access to human pancreas to generate human ECM as well as more defined characteristic of ECM molecules.

Another strategy to improve islet health post-bioprinting is the use of supporting cells together with islets in scaffold. Several studies have indicated that the addition of supporting cells such as mesenchymal stromal cells (MSCs), or endothelial cells to islet culture can improve islet function and survival.^[39] Co-axial bioprinting of islets in core of a tube-like scaffold and endothelial cells in the shell of the structure showed survival of the cells 21 days post-printing.^[40] Bioprinting rat islets together with endothelial cells reported reduced apoptosis and an increase in the expression of ECM molecules and VEGF analyzed by transcriptomics.^[41] Although, these studies suggested the beneficial effect of endothelial cells on islets post-bioprinting, they lack functionality analysis of islets in both in vivo and in vitro settings. MSCs are found in tissues such as bone marrow, adipose tissue and among other tissue types.^[42] Presence of MSCs together with islets has been reported to improve islet function by inducing the beneficial effect on islet glucose response and viability.^[43,44] Adipose-derived stromal cells (ASCs) can be easily isolated through minimal invasive lipoaspiration procedure and expanded to the larger amount. They have been investigated on various cell-based therapies and wound healing applications over the years.^[45–48] Similar to MSCs, the secretome and molecular properties of ASCs exhibit several favorable features for supporting islet cells. In particular, the ASC secretome has been reported to contain high levels of vascular and intracellular adhesion molecules as well as a diverse range of cytokines and growth factors.^[49,50] Moreover, co-culture and co-transplantation of ASCs

L. P. Nogueira, H. J. Haugen
Institute for Clinical Dentistry
University of Oslo
Oslo 0317, Norway

D. Josefsen, H. Scholz
Section for Cellular Therapy
Radiumhospitalet
Oslo University Hospital
Oslo 0379, Norway

S. Krauss
Department of Immunology and Transfusion Medicine
Oslo University Hospital
Oslo 0372, Norway

P. Gatenholm
CELLHEAL AS
Sandvika 1337, Norway

with mouse islets showed prolonged portal graft survival, islet function and glucose tolerance in diabetic immunocompetent mice.^[50–52] In these experiments, the paracrine effects of ASCs through secretion of protective and anti-apoptotic factors have been suggested to be one of the key factors to improve islet function and viability.^[53,54]

Here, we report for the first time the bioprinting of a double-layered cell delivery scaffold for pancreatic islets and ASCs with the combination of alginate/NFC bioink. We characterized the diffusion kinetics of small molecules varying in size between 3 and 70 kDa, inside the scaffold along with rheology and glucose absorption analysis by our bioink to model the nutrient and insulin exchange potential. In the bioprinting of the scaffolds with cells, we combined primary mouse or human islets with human ASCs while creating the delivery scaffold using bioprinting technique and visualized the even distribution of islets inside the bioprinted scaffolds using micro-computed tomography (micro-CT). We report the beneficial paracrine effect of the ASCs on islet function and viability through indirect culture of islets and ASCs by bioprinting the cells to two separate layers within the scaffold. We show that human ASCs can improve the islet behavior and their long-term function during the 60 days of intraperitoneal (IP) transplantation into diabetic mouse model and after recovery of the scaffolds, the presence of the ASCs in the scaffolds 60 days post-IP transplantation. This two layer approach suggests a positive impact and long-term support of ASCs on islets, prolonging the islet viability and function in this transplantable 3D bioprinted scaffold model.

2. Experimental Section

2.1. Ethics

The use of human donor islets (2011/782) and human ASCs (2014/838) was approved by the Regional Committee for Medical and Health Research Ethics Central (REC) in Norway. In vivo experiments were approved by the Norwegian National Animal Research Authority (FOTS ID 10680) and performed according to the guidelines for care and use of laboratory animals published by the US National Institutes of Health (NIH Publication, 8th Edition, 2011), and Norwegian Animal Welfare Act. All animals were handled by an experienced animal technician at all times in a blinded fashion to exclude eventual bias caused by pre-existing knowledge about the experimental groups.

2.2. Cell Isolation and Cultivation

2.2.1. Human Donor Islets

Human islets from non-diabetic donors were obtained via the JDRF award 31-2008-416 ECIT Islet for Basic Research Program, and isolated as previously described^[55] from 2 male and 2 female non-diabetic brain-dead donors with average age 53 years (46–59 years) and a BMI ≈ 20 (23–29 kg m⁻²) after appropriate informed consent from relatives for multi-organ donation and use in research. Islet preparations with at least a purity of >80% were used in this study verified by digital imaging analysis and using dithi-zone staining.^[56] Equally sized islets were manually hand-picked

and distributed randomly among the experimental groups to ensure uniformity. Islets were cultured at 37 °C (5% CO₂) up to 48 h on petri dishes (Sterilin, Newport, UK) using CMRL 1066 medium supplemented with 10% human AB serum (Milan ANALYTICA, Rheinfelden, Switzerland), 1% penicillin/streptomycin, 10 mmol L⁻¹ HEPES (Life Technologies, Carlsbad, CA, USA) prior to the start of experiments.

2.2.2. Primary Mouse Islets

Mouse islets were isolated from 8–18 weeks old male Balb/c Rag 1^{-/-} mice (Taconic, Denmark) as previously described.^[57] Isolated mouse islets were cultured at 37 °C (5% CO₂) up to 24 h on petri dishes (Sterilin, Newport, UK) using RPMI-1640 (HyClone, Utah, USA) supplemented with 10% heat-inactivated fetal bovine serum (FBS), 1% penicillin/streptomycin, 10 mm Hepes and 1% L-glutamine (Gibco, Paisley, UK) at 37 °C (5% CO₂) prior to the start of experiments.

2.3. Primary Human ASCs

Human ASCs were derived from healthy surgical adipose tissue excision samples (Oslo University Hospital, Norway, REC approval 2014/838 with informed consent obtained from individuals). Cells were isolated as previously described.^[47] Cells from all batches demonstrated the expressions of MSC-specific cell surface markers such as CD45, CD34, CD19, CD11b, or HLA-DR and they showed the ability to differentiate into cholangiocytes, osteocytes, and adipocytes after 14 days stimulation with specific culture medium.^[58,59] The same batch of cells as characterized was used in this study. All ex vivo expanded ASCs were used between passages 2 and 4. The cells were maintained in T175 cm² flasks ((Nunc; Thermo Fisher Scientific, Waltham, MA, USA) at 37 °C (5% CO₂) in essential medium MEM- α (Gibco, Thermo Fisher Scientific, Oslo, Norway) supplemented with 5% human platelet lysate (HPL) (Sexton Biotechnologies, USA), and 50 μ g mL⁻¹ gentamicin (Braun, Esbjerg, Denmark) prior to the start of experiments.

2.4. 3D Bioprinting of the Cell Delivery Scaffold

A double-layered scaffold with the size of 10 mm \times 10 mm \times 1 mm was designed using TinkerCAD web application and the resulting STL files were converted with Slic3r slicing program into G-code and manually adjusted to match the final intended format. Commercially available CELLINK Bioink (CELLINK AB), which is a mixture of 80% plant-derived NFC and 20% alginate, was used for bioprinting.^[30]

Prior to bioprinting, ASCs were trypsinized and collected by centrifugation (400 g, 8 min) before mixing them into the alginate/NFC bioink. An average of 1.2×10^6 ASCs per bioprinted scaffold (14×10^6 ASCs/1 mL bioink for about 12 scaffolds) was aimed since the previously published data showed good viability and function of cells with this density in the scaffolds.^[20,60] Hand-picked equally sized islets (100 human or mouse islets/scaffold) were added using PE-50 tubing and Hamilton threaded plunger

syringe and gently mixed with bioink using a small spatula on a sterile petri dish.^[60] Bioprinting was done using a pneumatic extrusion bioprinter INKREDIBLE+ (CELLINK AB) at a printing pressure of ≈ 5 –12 kPa for all layers, which is tolerable for most cells types and the size of the nozzles suitable for the size of islets and ASCs is selected to avoid excessive shear stress on the embedded cells.^[17,29] First, a solid ASC containing base layer was deposited using a blue standard conical 22 G (410 μm) nozzle. Subsequently, an islet containing layer consisting of an orthogonal grid of fibers was created with a pink standard conical 20 G (580 μm) nozzle. Calcium chloride (CaCl_2) solutions at a concentration of 50 mM (CELLINK AB) was used to crosslink and stabilize the final-obtained scaffolds right after bioprinting procedure for 5 min at room temperature. 3D bioprinted scaffolds were divided into four groups; i) mouse islets and human ASCs (mIslets+hASCs), ii) mouse islets alone (mIslets-alone), iii) human islets and human ASCs (hIslets+hASCs), and iv) human islets alone (hIslets-alone). All bioprinted samples were cultured in MEM- α complemented with 10% HPL, 1% penicillin/streptomycin, 10 mmol L⁻¹ HEPES (Life Technologies, Carlsbad, CA, USA).

2.5. Micro-CT Imaging

Phosphotungstic acid (PTA), which acts as an enhancer of contrast in micro-CT imaging,^[61] was used at the concentration of 0.3% PTA aqueous solution overnight at room temperature to stain and visualize islets inside the printed scaffolds. 100 islets/scaffold were used for this analysis. The scaffolds were placed into Eppendorf tubes for 3D x-ray imaging using a micro-CT Bruker 1172 system (Kontich, Belgium). Samples were scanned at 55 kV and 170 μA , with an exposure time of 250 ms per projection and a frame averaging of 4, leading to a total of 1000 ms per projection. In total 539 projections were acquired around 180°+ at an 1100 \times 1332 pixels (W \times H) field of view. The datasets were used for image reconstruction using NRecon (Bruker micro-CT version 1.7.5.9) software, and further segmentation and analysis was performed using Dragonfly software (version 2020.2, Object Research Systems (ORS) Inc., Montreal, Canada). For further info check Electronic Supplementary Method (ESM).

2.6. Fluorescence Recovery after Photobleaching (FRAP)

Cell-free circular alginate/NFC discs ($\varnothing 20$ mm) were generated and crosslinked as described earlier. The resulting discs were incubated at room temperature using varying sizes of 0.1 mg mL⁻¹ FITC-labelled dextran molecules (3–5, 10, 20, or 70 kDa (Sigma-Aldrich)) in PBS with 20 mM CaCl_2 (Sigma) overnight. 20 mM CaCl_2 was needed to keep the integrity of the scaffolds throughout analysis. FRAP was performed on 5 random spots per hydrogel disc using a Leica TCS SP8 STED confocal microscope with a 60 μm diameter bleaching area, and a frame rate of 0.223 s for 120 s. Fluorescence recovery curves were obtained from the collected imaging data using open source FIJI software (<https://fiji.sc/>). The time required for a bleached spot to recover half of its fluorescence intensity, halfway the recovery curve ($\tau_{1/2}$), was

determined with the help of FRAPbot software (<http://frapbot.kohze.com/>). Apparent diffusion constants (D) were determined according to Soumpasis et al. utilizing formula (1), with r the radius of the laser spot.^[62,63]

$$D = 0.224 \frac{r^2}{\tau_{1/2}} \quad (1)$$

2.7. Glucose Absorption Test

3D bioprinted cell-free alginate/NFC scaffolds were immersed in 30 mM glucose solution containing 20 mM CaCl_2 as a crosslinker and incubated in this solution for 60 min. Glucose level was measured via sampling before start of the incubation (0 min) and after 5, 15, 30, and 60 min post-incubation by using Glucose Colorimetric Detection Kit (Invitrogen, Oslo, Norway).

2.8. Rheology

All rheology measurements were performed with a Discovery HR-2 hybrid rheometer and 8 mm flat parallel plate geometry both from TA instruments. 1 mL of cell-free alginate/NFC hydrogel was filled into 12 mm diameter silicon molds and crosslinked with 50 mM calcium chloride for 5 min. Crosslinked discs were loaded into the rheometer. A solvent trap filled with distilled water was used to prevent hydrogels from drying. Hydrogels were preconditioned with a 5 min time sweep at 1% strain and an angular frequency of 10 rad s⁻¹. Followed by a frequency sweep at 1% and frequencies ranging from 0.1–600 rad s⁻¹ to determine a suitable frequency for the strain sweep. Last a strain sweep with strains ranging from 0.1–1000% strain and an angular frequency of 10 rad s⁻¹ were performed to determine the linear viscoelastic region of the hydrogel. The storage modulus within the linear viscoelastic region of the strain sweep was used to calculate the hydrogel mesh size utilizing formula (2).

$$D_{\text{mesh}} = \left(\frac{6 RT}{\pi N_{\text{av}} G'} \right)^{\frac{1}{3}} \quad (2)$$

2.9. Glucose Stimulated Insulin Secretion (GSIS) Assay

Human and mouse islet scaffolds with/without (w/wo) ASCs were incubated in Krebs buffer (11.5 mmol L⁻¹ NaCl_2 , 0.5 mmol L⁻¹ KCl, 2.4 mmol L⁻¹ NaHCO_3 , 2.2 mmol L⁻¹ CaCl_2 , 1 mmol L⁻¹ MgCl_2 , 20 mmol L⁻¹ HEPES, and 2 mg L⁻¹ albumin: all Sigma-Aldrich, Oslo Norway) containing 1.67 mmol L⁻¹ glucose for 2 h at 37 °C, followed by 2 h incubation in Krebs buffer containing 20 mmol L⁻¹ glucose, and again 2 h incubation with Krebs buffer containing 1.67 mmol L⁻¹ glucose. In parallel, GSIS analysis was also performed on 100 free-floating hand-picked equally sized human and mice islets in a similar manner except for a 45 min incubation time with each glucose/krebs buffer solutions instead of 2 h incubation time. It was assumed that a longer incubation of bioprinted cells was needed to compensate for the limitations in mass transport caused by the hydrogel. Insulin secretion was analyzed using either a human-specific or mouse-specific insulin ELISA kit (Mercodia, Uppsala,

Sweden). The stimulation index (SI) was calculated as a ratio of insulin secreted at high glucose (20 mmol L⁻¹) versus low glucose (1.67 mmol L⁻¹) indicating the glucose responsiveness of the islets.

2.10. Cell Survival after Bioprinting

The viability of cells after printing was assessed at day 1, 8, and 14 post-print using a standard live/dead assay based on fluorescein diacetate (FDA) 20 µg mL⁻¹ (Sigma-Aldrich, Oslo, Norway) and propidium iodide (PI) 100 µg mL⁻¹ (Thermo Fisher Scientific). Scaffolds were incubated with the live/dead staining solution containing 20 mM CaCl₂ for 5 min at room temperature before proceeding to imaging. Addition of CaCl₂ prevented disintegration of the samples by protecting the alginate ionic crosslinking. Scaffolds were imaged using an Axio Observer Inverted Microscope (Carl Zeiss AS) operated by ZEN lite software. 5 images per scaffold were taken at each time-point.

Cytotoxicity was determined by measuring the amount of mitochondrial Adenylate Kinase (ADK) in culture medium harvested at 1, 8, and 14 days using a ToxiLight non-destructive cytotoxicity bioassay kit according to the manufacturer's protocol (Lonza, Basal, Switzerland).

2.11. Biochemical Measurements

The level of mouse and human monocyte chemoattractant protein-1 (MCP-1, also known as CCL2), interferon gamma-induced protein-10 (IP-10, also known as CXCL10) and growth-regulated protein-α (GRO-α, also known as CXCL1) were measured in culture medium of bioprinted scaffolds at day 1, 8, and 14 post-print using a Procartaplex multiplex immunoassay according to the manufacturer's protocol (Thermo Fisher, MA, USA).

2.12. In Vivo Transplantation of Scaffolds

Animals were housed with no more than 5 mice per cage, under a 12 h light-dark cycle with free access to food and water except during fasting. Prior to transplantation experiments, diabetes was induced in 8–10 weeks old male BALB/c Rag 1^{-/-} immunodeficient mice (C.129S7(B6)-Rag1^{tm1Mom} J⁻¹, stock 003145, The Jackson Laboratory, Sacramento, California, USA) by administration of one dose of Alloxan Monohydrate (75 mg kg⁻¹) intravenously (Sigma Aldrich, Oslo, Norway) 3 days prior to transplantation of scaffolds to the IP or islets under the kidney capsule. Mice with non-fasting blood glucose ≥20 mmol L⁻¹ for 2 consecutive days were selected as viable diabetic recipients. For in vivo studies, scaffolds containing mIslets+hASCs or mIslets-alone (in each scaffold, 100 mouse islets and 1.2 × 10⁶ human ASCs) were transplanted at the IP site of the diabetic mice. In addition, 250 hand-picked free-floating mouse islets of the same islet batch were transplanted under the left kidney capsule as controls to verify the primary islet function.^[57] For experimental conditions, 6 mice were used in the mIslets+hASCs and mIslets-alone groups. In control experiments, 2–3 mice were used in the diabetic, non-diabetic and kidney capsule transplantation groups.

The mice were followed by measuring non-fasting blood glucose levels every 2 to 3 days randomly until the end of the experiment. At termination of studies on day 60, fasting blood glucose was measured and mice were sacrificed under anesthesia by a heart puncture for blood sampling and further analysis of mouse-specific C-peptide. In addition, mouse pancreases were snap frozen and stored in liquid nitrogen for analysis of remaining residual native beta cells.^[57] Transplanted scaffolds and islet grafts under kidney capsule were explanted also at termination of studies for further snap freezing and immunofluorescent microscopy imaging.

2.13. Immunofluorescent Imaging of Bioprinted Scaffolds

All explanted scaffolds were fixed in 4% paraformaldehyde, incubated overnight in 30% sucrose, followed by an overnight incubation in 60% sucrose/optimal cutting temperature compound (OCT compound) solutions. 20 mM CaCl₂ were added to all solutions before embedding in OCT. Using a cryo-microtome, 8 µm sections made and labelled with a mouse anti-human CD105 1:100 (Thermo Fisher Scientific Cat# MA5-11854, RRID:AB_10985671, Oslo, Norway) and guinea pig anti-mouse insulin 1:100 (Abcam, Cat# ab30477, RRID:AB_726924, Cambridge, UK) antibodies. Alexafluor 594 labeled donkey anti-mouse (Thermo Fisher Scientific Cat# A-21203, RRID:AB_141633, Oslo, Norway) and Alexafluor 488 goat anti-guinea pig (Thermo Fisher Scientific Cat# A-11073, RRID:AB_2534117, Oslo, Norway) antibodies, dilution ratio 1:300, were used as secondary antibodies while a nuclear staining using a SlowFade Gold antifade reagent with DAPI (Life Technologies AS, Oslo, Norway) was done as a counterstaining. Fluorescent light micrographs were taken, 5 representative locations per transplant, with an Axio Observer Inverted Microscope (Carl Zeiss AS) operated by ZEN lite software.

2.14. Statistical Analysis

Data are presented as mean ± SD. Differences among 3 study groups and more were evaluated by one-way ANOVA with Bonferroni corrections. A Mann–Whitney *U* test was performed for difference analysis between 2 groups. Significance was set at *p* < 0.05. Data were analyzed using GraphPad Prism software, version 6.0 (La Jolla, CA, USA).

3. Results

3.1. Even Distribution of Islets and ASCs after Bioprinting in Double-Layered Scaffold

Schematic image of the 3D bioprinted scaffolds created by Autodesk Fusion 360 shows our double-layered scaffold with the pancreatic islets in the top grid layer and ASCs in the bottom layer of the scaffold (Figure 1a). In order to investigate the number and the distribution of islets in bioprinted scaffolds, we developed a phosphotungstic acid (PLA) staining and micro-CT analysis method to visualize the islets post-printing within the

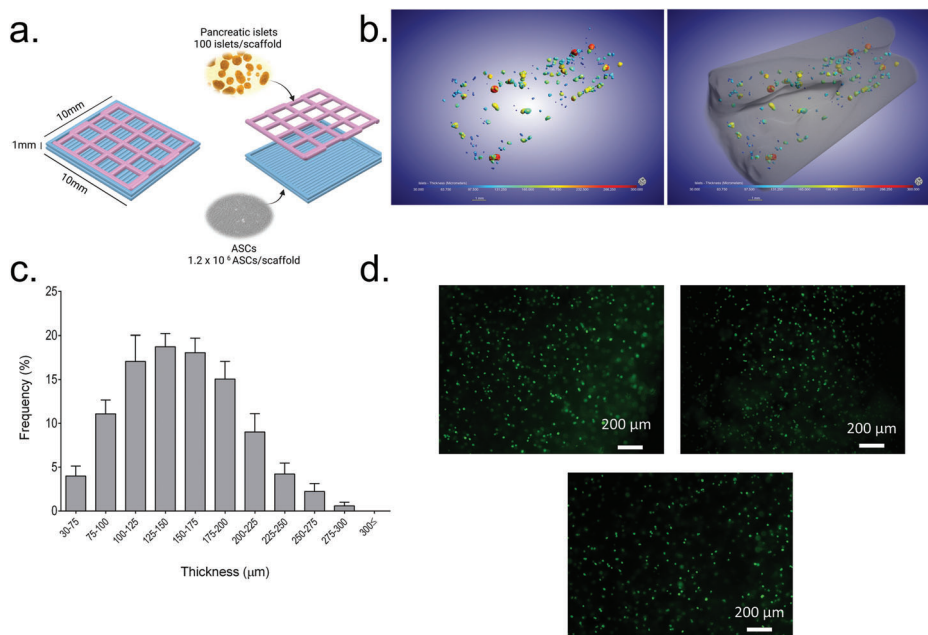


Figure 1. Schematic image of the 3D bioprinted scaffold as well as micro-CT and FDA imaging of islets and ASCs inside bioprinted scaffolds. a) Double-layered 3D bioprinted scaffold with pancreatic islets in the top layer and ASCs in the bottom layer, b) homologous distribution of islets within the scaffolds post-bioprinting, c) Image analysis shows that the frequency of islet size in each scaffold. d) Fluorescein diacetate (FDA) staining show the distribution of ASCs in scaffolds post-printing. $**p < 0.01$, $***p < 0.001$ versus 30–75 μm.

scaffolds. Micro-computed tomography (Micro-CT) imaging of human islets after bioprinting showed a homologous distribution throughout the delivery scaffold (Figure 1b, ESM, Electronic Supplementary Figure (ESF) 1, Electronic Supplementary Video (ESV) 1, and Electronic Supplementary Table (EST) 1, Supporting Information). Islet size in each scaffolds were ranged from 30 to 300 μm shown by different colors in which the blue indicates smaller islets and the red indicates larger islets (Figure 1b). In addition, we showed that most of the islets in bioprinted scaffolds were 100–200 μm in diameters (Figure 1c). Due to the small size of ASCs which were not visible in micro-CT, we performed FDA staining post-printing to show the distribution of the ASCs. This FDA staining of ASCs showed even distribution of the cells within the scaffolds post-printing (Figure 1d).

3.2. Alginate/NFC Bioink Was Able to Mass Transport Molecules with Different Sizes

FRAP is a technique which can be used to study the diffusion behavior of fluorescently labeled molecules. FRAP measures the speed of fluorescent molecule recovery in an optically transparent environment like a hydrogel after a specific area has been bleached by a confocal laser. We used a series of FITC-dextran molecules, ranging from 3–5, 10, 20 to 70 kDa, as defined model for insulin and other relevant biomolecules, which were incorporated into circular cell-free alginate/NFC bioink discs. A small spot of Ø 60 μm, inside these discs was subjected to bleaching by a confocal laser and fluorescence recovery over time was subsequently monitored using fluorescent confocal microscopy (Figure 2a–d, and ESV 2–4, Supporting Information) to determine diffusion kinetics of the different sized molecules through

the alginate/NFC bioink. Evaluation of the diffusion coefficients calculated from the FRAP data sets of different sized dextran molecules show that the diffusion rate of 3–5 kDa FITC-labeled dextran is significantly higher than 20 and 70 kDa (Figure 2e,f). Overall, the fluorescent intensity of the bleached spots recovered for all molecules around 1 min (Figure 2e). This indicates that although the rate of diffusion decreases with the size of the dextran molecule, eventually all molecules were able to diffuse through the bioink. The fluorescence recovery curves clearly show that the diffusion rate of larger sized molecules is much lower than of the smaller sized molecules, indicating that the bioink is limiting free diffusion of molecules depending on their size. By performing a strain sweep and determining the storage modulus G' (ESF 2a,b, Supporting Information), we also calculated the average mesh size (D_{mesh}) of our bioink which was $6.35 \text{ nm} \pm 0.5 \text{ nm}$ (EST 2, Supporting Information). Due to the importance of glucose on islet function, we also investigated the rate of glucose absorption from the surrounding glucose solution into the 3D bioprinted cell-free scaffold. Our data report the absorption of glucose by the biomaterial until 30 min post-incubation in glucose solution before it reached plateau (ESF 3, Supporting Information). Following the FRAP and rheology analysis, this analysis also shows the ability of our biomaterial to absorb small molecules.

3.3. Human ASCs Improved the Function and Viability of Mouse Islets in Bioprinted Scaffolds

Double-layered scaffolds were bioprinted with either mouse islets or a combination of mouse islets and human ASCs to determine the islet function at different time points after printing. GSIS

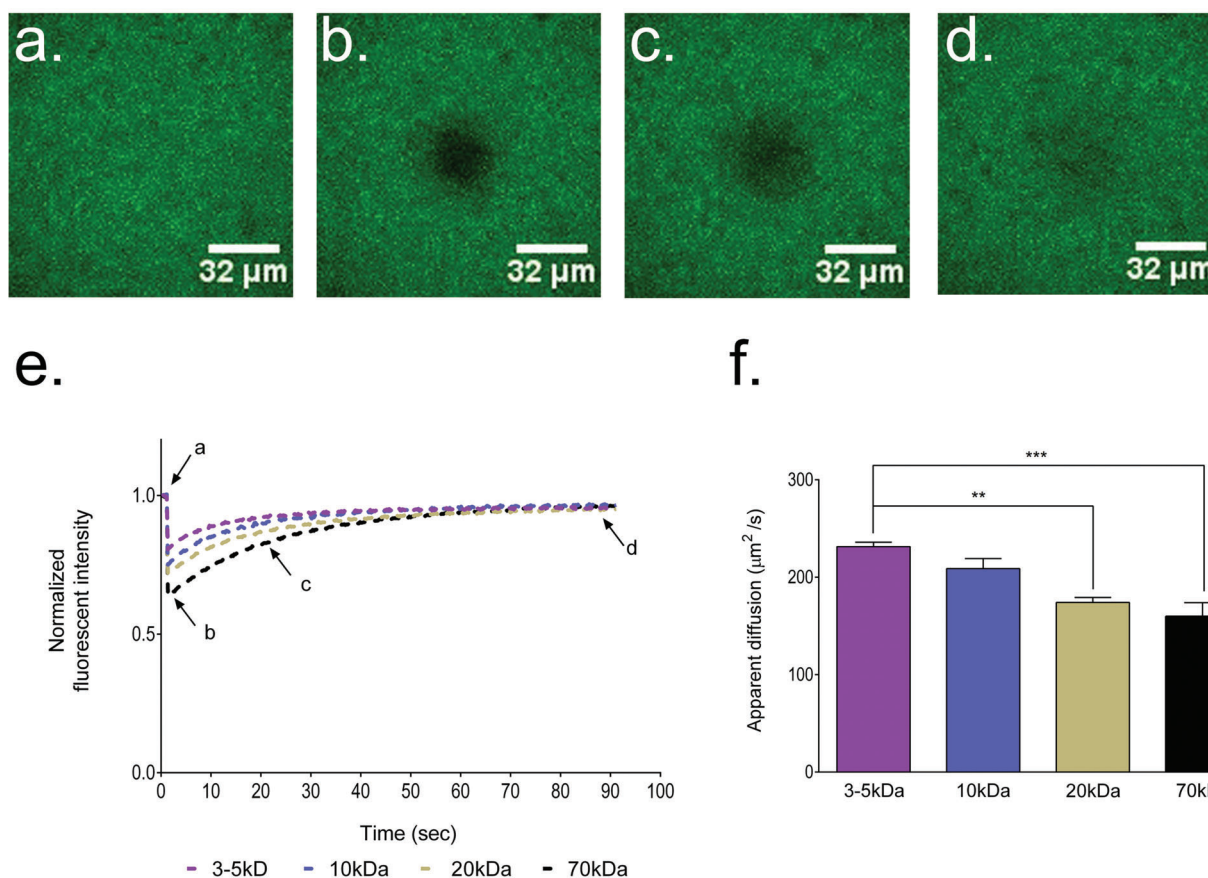


Figure 2. Diffusion of various sized molecules in alginate/NFC bioink. a) Confocal images of the bioprinted alginate/NFC discs saturated with fluorescent-labelled dextran molecules of 3–70 kDa in size, before bleaching, b) during bleaching, c) early recovery phase, and d) late-recovery phase. e) The fluorescence recovery curves were obtained by determining fluorescence intensity of the bleached area of each dextran molecule in separate discs made from alginate/NFC. f) The fluorescence recovery curves were used to calculate the rate of diffusion (apparent diffusion). All printed discs were measured five times at random locations. Data are presented as mean \pm SD analyzed by one-way ANOVA with Bonferroni corrections. $**p < 0.01$ and $***p < 0.001$ versus 3–5 kDa.

was performed at day 1, 8, and 14 post-bioprinting. Although, insulin secretion in response to high glucose levels (20 mM) increased in the mIslets-alone, islets in this group failed to reduce insulin secretion to basal levels during the second incubation in low glucose (1.67 mM) solution (Figure 3a). In contrast, bioprinted mIslets+hASCs showed an increase in insulin secretion in response to 20 mM glucose and a normal return to basal levels at all analyzed time points. In parallel, GSIS analysis on free-floating mouse islets also showed an increase in insulin secretion in response to high glucose levels on day 1 post-isolation, which was followed by the return of insulin levels to basal levels by switching to low glucose solution (Figure 3a). In addition, we found a significant increase in SI levels in mIslets+hASCs group on day 1 and 14 post-bioprinting compared to the mIslets-alone group (day 1 post-bioprinting, mIslets+hASCs 2.581 ± 0.14 vs mIslets-alone 1.108 ± 0.04 , $p < 0.05$, Day 8 post-bioprinting, mIslets+hASCs, 1.575 ± 0.05 vs mIslets-alone 1.108 ± 0.04 , Day 14 post-bioprinting, mIslets+hASCs 1.410 ± 0.06 vs mIslets-alone 0.7989 ± 0.1095) (Figure 3b). These data clearly show the impaired function of mIslets-alone group to return to basal insulin secretion levels, whereas, the islets function was improved in the presence of human ASCs (Figure 3b).

ADK is a well-known alternative to ATP and acts as a marker for cell death releasing from cells into the surrounding environment.^[64] Bioprinted mIslets+hASCs group showed a trend in reducing the levels of secreted ADK compared to the mIslets-alone group on day 1 and 8 post-bioprinting. A significant reduction in the levels of ADK was observed on day 14 post-bioprinting in mIslets+hASCs group compared to the mIslets-alone group (Figure 3c). In addition, fluorescence imaging of scaffolds revealed less PI positive cells in the mIslets+hASCs group compared to mIslets-alone group, which was in line with ADK data (Figure 3c,d).

3.4. Human ASCs Improved the Function and Viability of Human Islets in Bioprinted Scaffolds

In order to determine the human islet function post-3D bioprinting, double-layered scaffolds were bioprinted with either human islets or a combination of human islets and human ASCs. GSIS revealed that the overall insulin secretion increased in the hIslets-alone group over time; however, these scaffolds showed blunted insulin secretion when transferring them from high

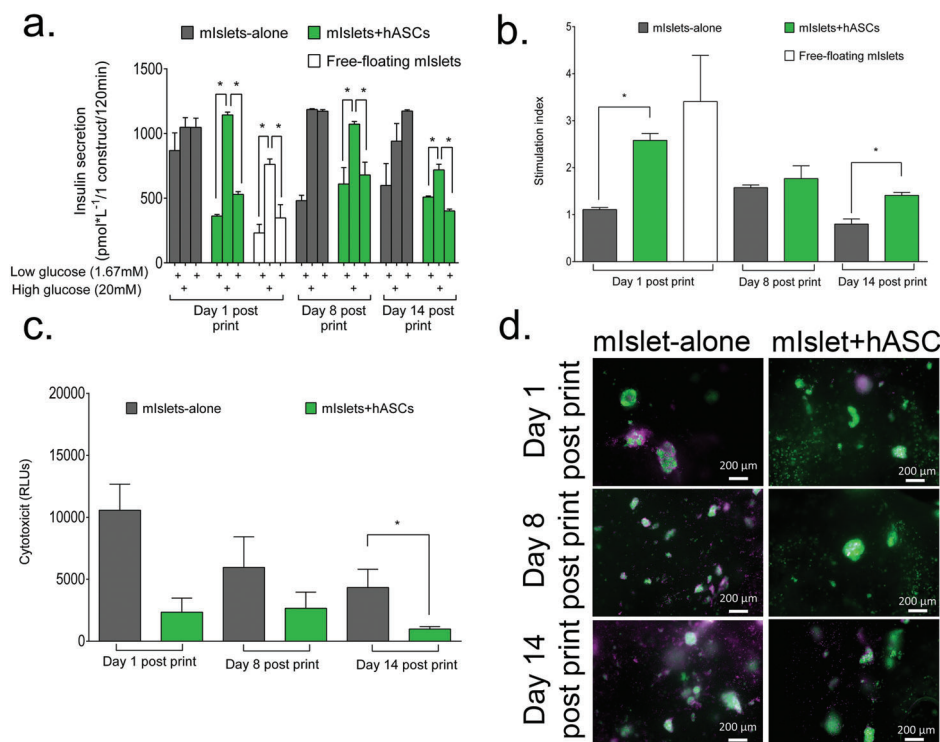


Figure 3. Human ASCs support glucose responsiveness and cell viability of mouse islets in biprinted scaffolds. a) Insulin secretion in response to basal (1.67 mM) and stimulated (20 mM) levels of glucose measured by b) ELISA and calculated as stimulation index for mouse islets w/o human ASCs analyzed at day 1, 8, and 14 post-bioprinting (a, b). c) Cell loss was measured via ADK released from degrading cells in biprinted scaffolds on day 1, 8, and 14 post-bioprinting. d) FDA (live cell-green)/PI (dead cell-purple) staining followed up by the visualization of mouse islets w/o human ASCs at day 1, 8, and 14 post-bioprinting. Scale bars 200 μ m, $n = 4$ independent biological replicates. Data are presented as mean \pm SD and analyzed by one-way ANOVA with Bonferroni corrections and Mann–Whitney U test. * $p < 0.05$ versus high glucose (20 mM) group, * $p < 0.05$ versus mIslets-alone group.

glucose levels (20 mM) to low glucose (1.67 mM) (Figure 4a). In contrast, biprinted hIslets+hASCs scaffolds showed proper maintenance of islet function during culture (Figure 4a). Free-floating human islets displayed reasonable insulin secretion albeit lower than in the hIslets+hASCs group at day 1 (Figure 4a). The hIslets+hASCs scaffolds displayed elevated levels of SI compared to the hIslets-alone group (Day 1 post-bioprinting, hIslets+hASCs 1.835 ± 0.22 vs hIslets-alone 1.239 ± 0.27 , Day 8 post-bioprinting, hIslets+hASCs, 2.408 ± 0.42 vs hIslets-alone 0.7203 ± 0.13 , Day 14 post-bioprinting, hIslets+hASCs 2.315 ± 0.38 vs hIslets-alone 0.7203 ± 0.13) (Figure 4b). In addition, biprinted hIslets+hASCs scaffolds showed lower levels of ADK compared to the hIslets-alone group over time. Moreover, fluorescence microscopy revealed less PI positive cells in the hIslets+hASCs group compared to the hIslets-alone group, which is in line with ADK data (Figure 4c,d).

3.5. Presence of Human ASCs in Islet Scaffolds Reduced Secretion of Pro-Inflammatory Cytokines

In order to study the inflammatory stress effect of 3D bioprinting process on the islets within the scaffolds, we measured secretion of three pro-inflammatory cytokines, which their secretions by islets have been reported post-clinical islet transplantation.^[65–67] We also investigated whether presence of ASCs in the scaffold

could induce a protective effect on the mouse and human islets. It has been previously reported that co-culture of human islets with human ASCs could reduce the secretion of the pro-inflammatory cytokines.^[49] In comparison to mIslets+hASCs biprinted scaffolds, mIslets-alone scaffolds showed in general higher mouse specific pro-inflammatory cytokine levels, at all analyzed time points (Figure 5). We found a significant decrease in secretion of measured cytokines in mIslets+hASCs group compared to the mIslets-alone group on day 1 post-bioprinting for all three cytokines and on day 14 post-bioprinting for GRO- α and IP-10 (Figure 5a–c, EST 3, Supporting Information). The same cytokine secretion reducing effect of human ASCs were observed in hIslets+hASCs group compared to the hIslets-alone group (Figure 5d–f, EST 4, Supporting Information). We observed a significant decrease of human GRO- α and MCP-1 on day 1 post-bioprinting and IP-10 on day 8 post-bioprinting in hIslets+hASCs group compared to the hIslets-alone group (Figure 5d–f, EST 4, Supporting Information).

3.6. Mitigation of Diabetes Influenced by Human ASCs in 3D Bioprinted Islet Scaffolds

To assess the effect of human ASCs on islet function and glucose regulation in vivo, mIslets+hASCs scaffolds were transplanted to the IP site of the diabetic mice and followed up for 60 days

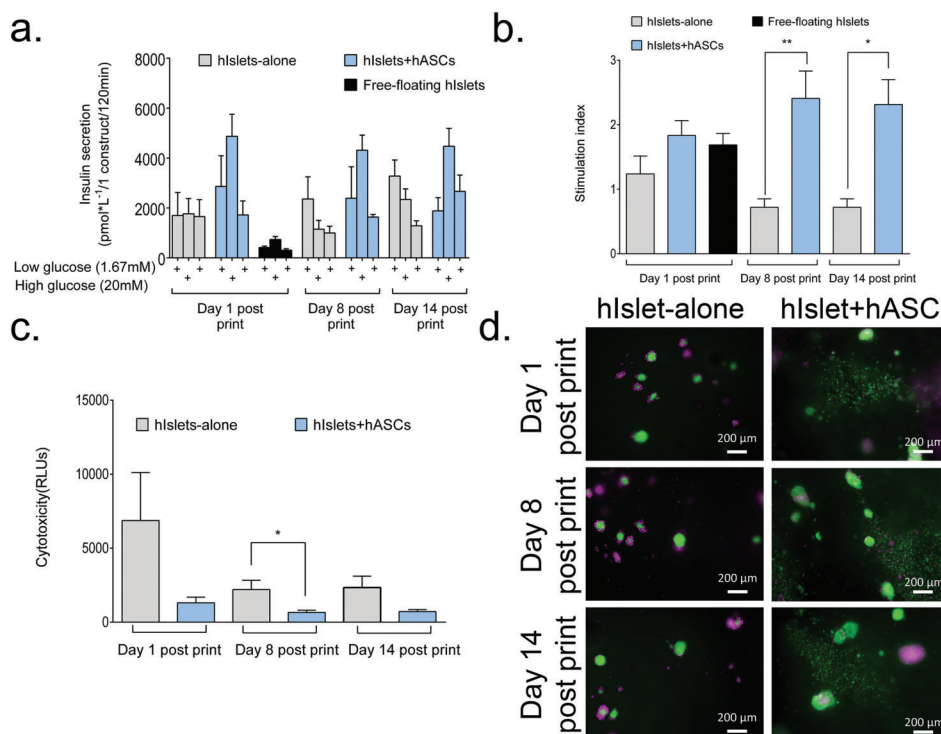


Figure 4. Human ASCs support glucose responsiveness and cell viability of human islets in bioprinted scaffolds. a) Insulin secretion in response to basal (1.67 mmol L⁻¹) and stimulated (20 mmol L⁻¹) levels of glucose measured by ELISA and calculated as b) SI for human islets w/o human ASCs analyzed at day 1, 8, and 14 post-bioprinting. c) Cell loss was measured via ADK released from degrading cells in bioprinted scaffolds at day 1, 8, and 14 post-bioprinting. FDA (live cell-green)/PI (dead cell-purple) staining followed up by the visualization of human islets w/o ASCs at day 1, 8, and 14 post-bioprinting (d). Scale bars 200 μm, *n* = 4 independent biological replicates. Data are presented as mean ± SD and analyzed by Mann–Whitney *U* test. **p* < 0.05 and ***p* < 0.01 versus the hIslets-alone group.

post-transplantation. All animals transplanted with scaffolds containing mouse islets showed a reduction in blood glucose and reaching normoglycemia (10 mm blood glucose) around day 7 (Figure 6a,b). However, blood glucose in diabetic mice with scaffolds containing mIslets+hASCs clearly displayed less fluctuation over time and was always under the 10 mm threshold, while mice with mIslets-alone scaffolds remained above this threshold (Figure 6a,b). Kaplan–Meier curves indicate that the time until normoglycemia was reached around day 7 for mIslets+hASCs scaffolds, whereas for mIslets-alone scaffolds, the time of reaching normoglycemia was at the end of the transplantation period at day 56 (Figure 6c). To compare the 3D bioprinted scaffolds with the gold standard in vivo potency bioassay, 250 free-floating mouse islets were transplanted under kidney capsule of the diabetic mice as control animal group. In these control animals, the reduction in blood glucose to normoglycemic levels was observed from day 2 post-transplantation, which was similar to mice treated with the bioprinted mIslet+hASCs scaffolds (Figure 6c). This outcome indicates that the 100 primary mouse islets within the scaffold benefit from the presence of ASCs to reach stable normoglycemia in a relatively short time similarly to the control group where the 250 islets were transplanted under the kidney capsule. Whereas the diabetic mice transplanted with mIslet-alone scaffolds needed considerably longer time to reach normoglycemia and seemed to be less effective.

The measurement of circulating C-peptide and the ratio of C-peptide to fasting blood glucose have been known as the sign of

preserved islet function post-transplantation.^[68] C-peptide measured on day 60 showed a significant increase in mice transplanted with the mIslets+hASCs scaffolds compared to the mIslets-alone group (Figure 6d). C-peptide levels in these mice were similar to mice transplanted with islet grafts under kidney capsule, while mIslets-alone transplanted mice displayed significantly lower levels of secreted C-peptide (Figure 6d). Similarly, the ratio of mouse C-peptide to fasting blood glucose in mice transplanted with mIslets+hASCs scaffold was significantly higher compared to mice transplanted with mIslets-alone scaffolds on day 60 post-transplantation (Figure 6e). Control analysis of native insulin in mouse pancreata showed no detectable insulin, indicating that no significant beta cell regeneration had taken place during the transplantation period (ESF 4, Supporting Information). This confirms that C-peptide was secreted by the transplanted islets in the scaffolds. Explanted mIslets+hASCs scaffolds showed insulin and CD105 positive cells for beta cells and ASCs respectively, indicating the presence of both islets and ASCs in the transplanted scaffolds 60 days post-transplantation (Figure 6f).

4. Discussion

In this study, we present a method for 3D bioprinting of transplantable alginate/NFC scaffold that contains mouse or human islets together with ASCs as supportive cells for islet function.

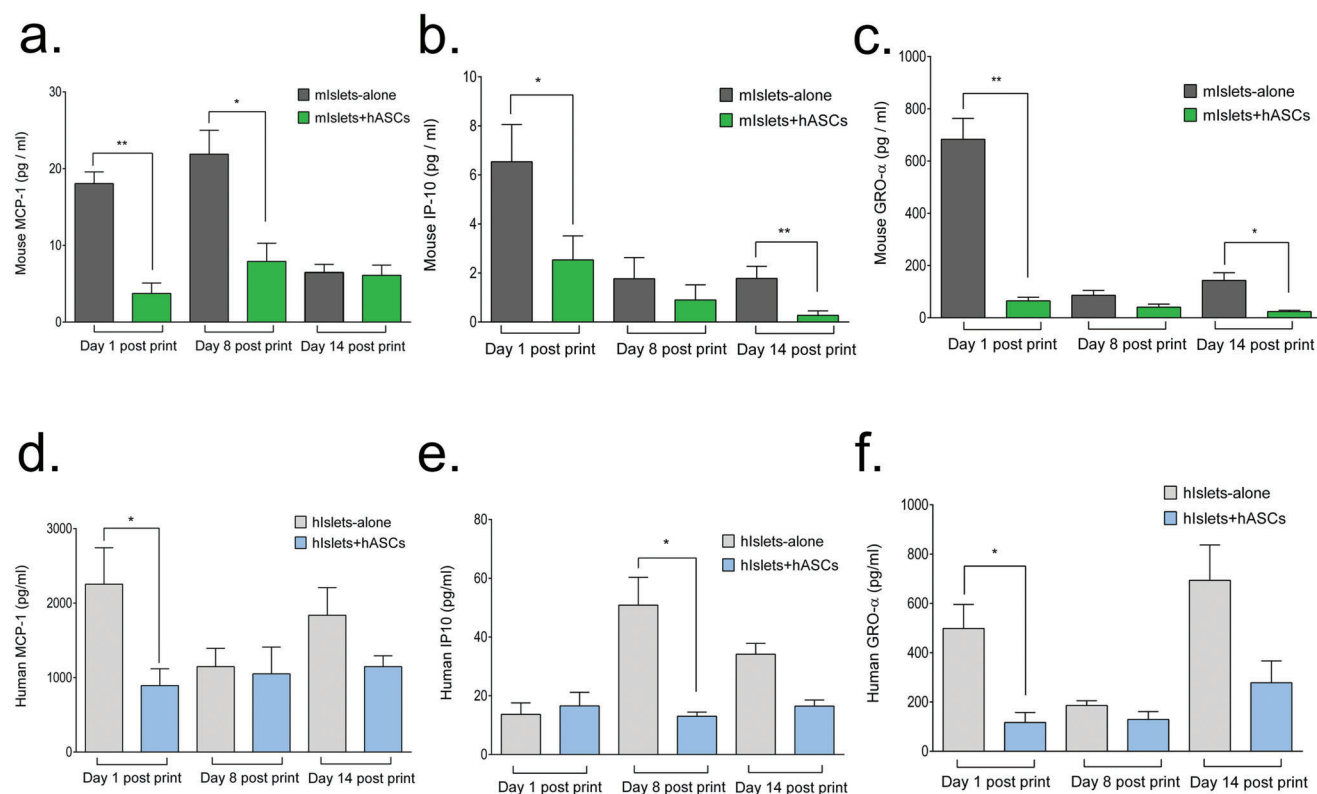


Figure 5. Comparison of inflammatory cytokine releases from bioprinted islet scaffolds w/o human ASCs. The assessment of the mouse inflammatory cytokines a) MCP-1, b) IP-10, and c) GRO- α in bioprinted scaffolds containing mouse islets and human ASCs at day 1, 8, and 14 post-bioprinting. Data are presented as mean \pm SD and analyzed by a Mann-Whitney U test, $n = 4$ independent biological replicates, * $p < 0.05$, and ** $p < 0.01$ versus hlslets-alone scaffolds. The assessment of the human inflammatory cytokines d) MCP-1, e) IP-10, and f) GRO- α in bioprinted scaffolds containing human islets and human ASCs at day 1, 8, and 14 post-bioprinting. Data are presented as mean \pm SD and analyzed by a Mann-Whitney U test, $n = 4$ independent biological replicates. * $p < 0.05$ versus hlslets-alone group.

Transplanting pancreatic islets to alternative extrahepatic sites can play an important role in improving the outcome of beta cell replacement therapy.^[69] Tissue engineering technologies such as 3D bioprinting offer advanced and versatile tools for the creation of transplantable islet scaffolds and delivery devices that can be used toward development of modern T1D treatment options.^[8,70] Despite the significant progress in the development of islet delivery macro-scaffolds, major challenges including the long diffusion pathway for nutrients and oxygen to reach the islets as well as the number of cells per device have still remained unsolved.^[71]

Alginate as standing alone biomaterial with fast cross-linking ability and high water content offers fast exchange of nutrients, oxygen and waste throughout the 3D bioprinted scaffolds.^[72] However, alginate has poor printability but in combination with other hydrogels with higher printing fidelity, the printability can be improved. As previously shown, the combination of alginate with NFC offers desirable properties for bioprinting of living cells due to the suitable rheological properties for printing and encapsulation of cells, and additionally, the shear-thinning nature of the NFC that allows precise printability.^[29,73] Also, we previously reported about the stability of the bioink material where cell-free alginate/NFC scaffolds did not degrade, but stayed intact during 10 months of follow-up period post-transplantation in a mouse model.^[60] Similarly, very low levels of biodegradation of

alginate/NFC scaffolds have been reported after 10 months transplantation in an application with chondrocytes and chondrocytes together with MSCs in vivo.^[20,54] Following up with this data, the measurement of the diffusion properties of alginate/NFC bioink using FRAP analysis reported that the used bioink in this study allows the diffusion of wide-range of small molecules with the size from 3 to 70 kDa. This data together with the measured mesh size and glucose absorption by the bioink as an example show the ability of this bioink to exchange molecules with various sizes between the cells and outer environment. Previously published studies reported bioprinting and maintenance of liver cells and induced pluripotent stem cells (iPSCs) in alginate/NFC scaffolds.^[17,72] They showed that this bioink combination was suitable for keeping the pluripotency of iPSCs later used to generate cartilage tissue.^[74] Recently two studies has shown the use of tunicates that is another source of NFC, in combination with alginate as bioink to create 3D bioprinted scaffolds of human chondrocytes and autologous micro-fat for pre-clinical applications.^[16,75] These publications together with our data show the long-term stability and compatibility of the material as a transplantable biomaterial and more importantly also, show the suitable diffusion properties of vital nutrients as well as maintenance of encapsulated cells including islets post-bioprinting procedure.

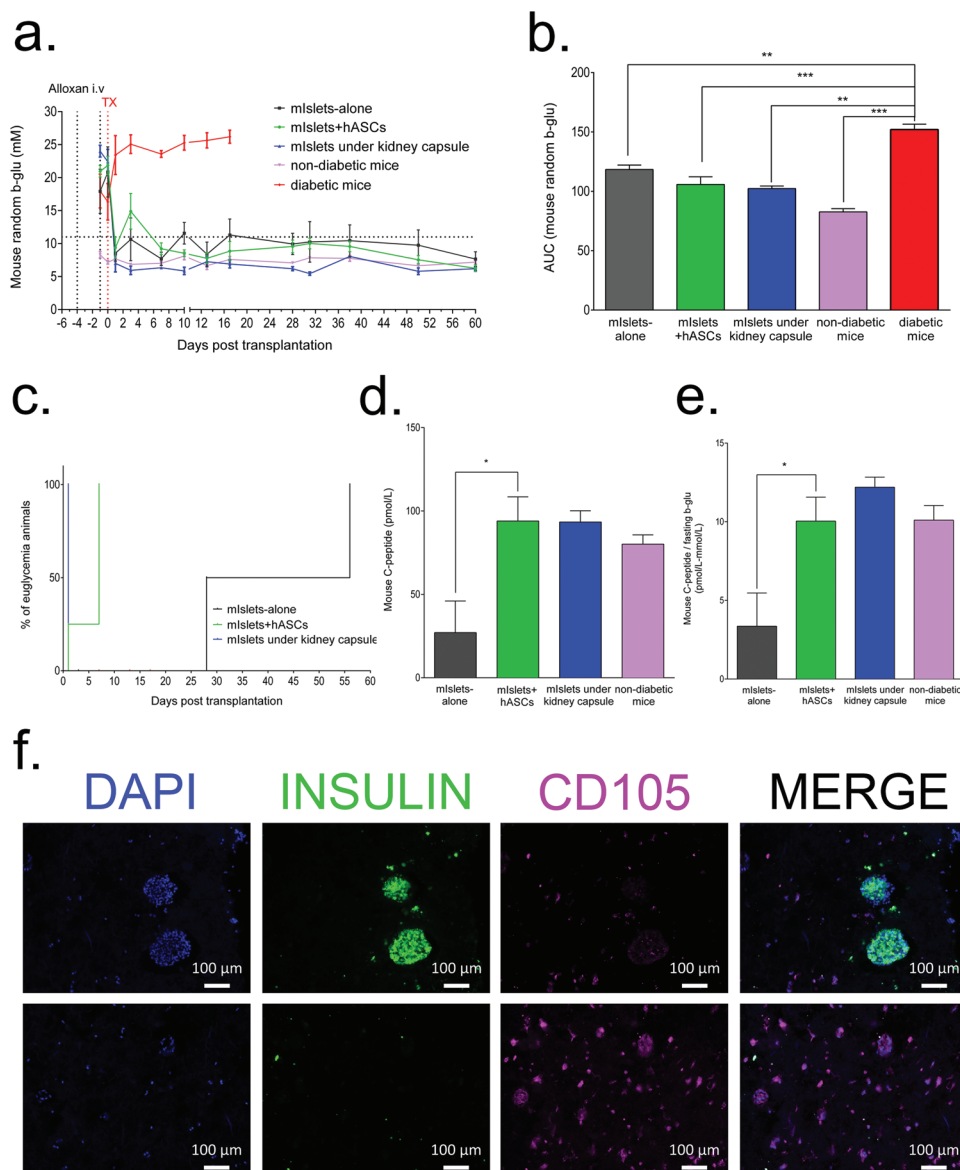


Figure 6. Improved in vivo efficacy of 3D bioprinted mIslets + hASCs in diabetic mice. Random blood glucose measurements over a) 60 days post-transplantation and b) calculated AUC in mice transplanted with mIslet scaffolds w/o ASCs. Islets transplanted under the kidney capsule, healthy and diabetic mice served as controls. c) Kaplan–Meier curves for mice transplanted with scaffolds or islet grafts under kidney capsule. d) Circulating mouse C-peptide and e) calculated ratio of mouse C-peptide to fasting blood glucose at the termination of studies for diabetic mice transplanted with either scaffolds or mouse islet grafts under kidney capsule. f) Immunofluorescent labeling of explants for insulin and CD105 at day 60 post-transplantation. Magnification 10 \times , scale bar 200 μ m. In all analysis, data are presented as mean \pm SD and analyzed by one-way ANOVA with Bonferroni corrections and unpaired Mann–Whitney U test, $n = 3$ independent biological replicates and for each replicate 6 mice per group were used. * $p < 0.05$ versus mIslets-alone group. ** $p < 0.01$ and *** $p < 0.001$ versus diabetic mice group.

The other major challenge with bioprinting of islet scaffolds is the knowledge of cells and their distributions within scaffolds. Pancreatic islets are metabolically active organoids that prefer sparse distribution in their native environment. Having them in close proximity with each other induce hypoxia and cellular stress signals that could negatively affect their function and viability.^[79] Therefore, the number of islets per scaffold and the islet positioning within the scaffold could have reducing impact on the long-term function of islets in scaffolds. Micro-CT imaging has been used previously to study the shape and the pore size of 3D bio-

printed scaffolds but not for identifying the number of cell clusters within a scaffold.^[77] Phase-contrast imaging using micro-CT with PTA staining has been shown to give high-quality visualization of chondrocytes in articular cartilage.^[61,78] By utilizing this technique, we were able to visualize islets post-bioprinting in the scaffolds and show that we have equally distributed islets in each scaffold.

During the islet isolation procedure, the islets go through both mechanical and enzymatic destructions of pancreatic tissue which results in disruption of islet micro-environment and

endocrine cell niche.^[79,80] This disruption has been reported to cause increased levels of some pro-inflammatory cytokines including IL-6, IL8 and MCP-1 post-islet isolation.^[81,82] We also reported elevated levels of the pro-inflammatory cytokines IP-10, GRO- α , and MCP-1 secreted by both human and mouse islets from islet-alone scaffolds post-bioprinting. The increase of these three measured mediators has previously been reported in the early phase after clinical islet transplantation in T1D patients.^[83–85] One strategy to improve islet health is to create a supportive micro-environment for the islets with ECM molecules and anti-inflammatory cytokines. One strategy to create this supportive micro-environment for pancreatic islets is bioprinting of islet scaffold with suitable bioink mixed with ECM proteins extracted from pancreatic tissue. Although, this strategy could be beneficial for the islets, challenges including purifying ECM proteins from the pancreatic tissue and characterizing all molecules of the ECM as well as potential access to human pancreas to isolate ECM make this strategy hardly applicable for clinical purposes.^[37] Therefore, we used ASCs as the source of ECM and growth factors that could be beneficial for 3D bioprinted islets. Our previous co-culture studies of islets and ASCs have shown the paracrine effects of ASCs for prolonging islet survival and function as well as reducing inflammatory reactions.^[49,52] Cell-free therapies by using ASC secretome from conditioned medium and ASC-derived extracellular vesicle have been considered also in various clinical trials for treatment of neurodegenerative, cardiovascular and metabolic diseases.^[86,87] However, challenges of the short half-life of these ECM molecules, growth factors, and cytokines as well as the frequencies of administration need more investigation for long-term outcome of these strategies.^[33,77,88,89] In addition, presence of the bioink in 3D bioprinted cell structures could make these strategies more complicated in terms of the absorption rate and the lag time for these factors reaching islets.

We printed islets and ASCs in two separate layers in a double-layered scaffold. The shape and geometry of the scaffold in this study have been tested previously with various types of cells. As previously published, 3D grid-like shaped scaffold containing chondrocytes and MSCs at the density of 1×10^6 cells per scaffold in alginate/NFC bioink showed proliferation of the cells as well as type 2 collagen and glycosaminoglycan by chondrocytes 60 days post-transplantation subcutaneously in nude mouse model.^[20,28] Another study using the similar 3D scaffold structure and similar number of cell density harvested from fat tissue (containing ASCs, endothelial progenitor cells, and endothelial cells) reported 150 days of scaffold survival in vivo as well as identifications of angiogenesis in nude mouse model.^[90] Although in these studies ASCs or MSCs were mixed together in the scaffold, direct co-culture or mixing of islets and ASCs can induce adhesion of ASCs on the islet surface. This can change the morphology of an islet and affect the potency of insulin secretion.^[91] However, indirect culture of ASCs on a petri dish and islets in transwells in close proximity has been reported to be beneficial through secretion of growth factors including Hepatocyte growth factor (HGF) and Vascular endothelial growth factor (VEGF) from ASCs to improve islet function.^[92] Our strategy in bioprinted ASCs and islets into a double-layered scaffold also serves as an indirect co-culture method of islets and ASCs that revealed reduction in secretion of IP-10, GRO- α and MCP-1 from bioprinted scaffolds. Thus,

ASCs could be an effective approach to improve the islet micro-environment and consequently islet health when using in tissue engineering constructs.

Although, bioprinting of islet scaffold has been reported previously, generation of transplantable islet scaffolds has been yet to achieve. Islet transplantation under kidney capsule is considered as the standard model to monitor the islet potency.^[93] A tissue engineered biomaterial based scaffold that is transplantable to an extrahepatic site and also easily retrievable, would give an invaluable knowledge and a possibility to monitor long-term islet function toward investigation of alternative and novel regenerative approaches for T1D treatment.^[94–96] In this study, we used our defined minimal mass of islets together with ASCs, to study the indirect effects of ASCs in the scaffolds. ≥ 200 mouse islets are considered a full islet mass that is required to achieve normoglycemia in allogenic diabetic mouse model.^[97,98] To study whether ASCs can improve minimal islet function under diabetic micro-environment, we bioprinted scaffolds containing 100 mouse islets and 1.2×10^6 human ASCs. Co-transplantation of ASCs with marginal allogenic islets under kidney capsule has also been reported to prolong graft survival in diabetic mice.^[52] The beneficial effect of ASCs is thought to improve islet function and their glucose responsiveness in vivo.^[49,50]

The transplantation of a scaffold to the IP site of a diabetic mouse model is beneficial due to the easy accessibility and the larger space for different shaped scaffolds as these strategies are developing toward clinical applications.^[99] However, delayed delivery of oxygen and nutrient supplies due to the passive diffusion properties compared to the kidney capsule site could hinder the outcome of transplanted scaffolds at the IP site.^[100] We used a dose of 1.2×10^6 human ASCs in the scaffolds transplanted at the IP site. Five-times intravenous administration of 5×10^6 ASCs to a diabetic mouse model has been shown to be less inefficient for reversal of diabetes. This was also confirmed by detection of ASCs in lungs, spleen and peritubular regions but not in the pancreas post-infusion.^[101] Interestingly, our immunofluorescent staining data shows the presence of ASCs together with islets in scaffolds for at least 60 days post-transplantation. Therefore, bioprinting ASCs together with islets could be advantageous strategy for keeping the beneficial indirect effects of ASCs on islets post-transplantation and support the preservation of islet function.

5. Conclusion

This is the first study showing the supportive role of ASCs on pancreatic islets specifically in 3D bioprinted scaffolds. The model exhibited the possibility of transplanting fewer islets together with ASCs to achieve normoglycemia and maintenance of it throughout the study time frame of 60 days. In addition, we demonstrated the stability of islet function and viability in vitro when bioprinted with ASCs to a scaffold up to 14 days. This study makes the ground for future research for moving the field of beta cell replacement therapy toward developing stem cell-derived islet-like organoids that could potentially replace allogenic human islet transplantation. Recreation of clinically relevant physiological islet micro-environment for these organoids could be achieved by using supportive cells and engineering

scaffolds that hold different cell types together for long-term engraftment using an extrahepatic transplantation site.

Supporting Information

Supporting Information is available from the Wiley Online Library or from the author.

Acknowledgements

The authors are grateful to all members at the human islet isolation facility at the Oslo University Hospital, Oslo, Norway. They especially thank Merete Høyem, Marina Katavic, and Ragnhild Fjukstad for technical expertise and helpful discussions. This work was supported by the Research Council of Norway through its Centre of Excellence funding scheme, project number 262613, The Norwegian Diabetes Association, Oslo Diabetes Research Center, Southern and Eastern Norway Regional Health Authority, project number 2019027 as well as Research Council of Norway, project number IPN 317790. S.A and H.S are the guarantors of this work, and as such have full access to all data in the study and take responsibility for the integrity of the data and the accuracy of the data analysis.

Conflict of Interest

P.G. is CEO of CELLHEAL AS, however CELLHEAL AS was not involved in the design of the study; the collection, analysis, and interpretation of data; writing the report; and did not impose any restrictions regarding the publication of the report. The remaining authors declare that there are no competing interests that could be perceived as prejudicing the impartiality of the research reported.

Data Availability Statement

The data that support the findings of this study are available from the corresponding author upon reasonable request.

Keywords

islets, 3D bioprinting, ASC, scaffolds, in vivo, alginate, nanocellulose

Received: February 27, 2023

Revised: September 7, 2023

Published online:

- [1] L. Piemonti, A. Andres, J. Casey, E. Koning, M. Engelse, R. Hilbrands, P. Johnson, B. Keymeulen, J. Kerr-Conte, O. Korsgren, R. Lehmann, T. Lundgren, P. Maffi, F. Pattou, F. Saudek, J. Shaw, H. Scholz, S. White, T. Berney, *Transplant Int.* **2021**, *34*, 1182.
- [2] B. Hirshberg, K. I. Rother, B. J. Digon, J. Lee, J. L. Gaglia, K. Hines, E. J. Read, R. Chang, B. J. Wood, D. M. Harlan, *Diabetes Care* **2003**, *26*, 3288.
- [3] T. Anazawa, H. Okajima, T. Masui, S. Uemoto, *Ann. Gastroenterol. Surg.* **2019**, *3*, 34.
- [4] E. A. Ryan, B. W. Paty, P. A. Senior, D. Bigam, E. Alfarhli, N. M. Kneteman, J. R. T. Lakey, A. M. J. Shapiro, *Diabetes* **2005**, *54*, 2060.
- [5] A. N. Balamurugan, R. Bottino, N. Giannoukakis, C. Smetanka, *Pancreas* **2006**, *32*, 231.

- [6] J. F. Markmann, M. R. Rickels, T. L. Eggerman, N. D. Bridges, D. E. Lafontant, J. Qidwai, E. Foster, W. R. Clarke, M. Kamoun, R. Alejandro, M. D. Bellin, K. Chaloner, C. W. Czarniecki, J. S. Goldstein, B. J. Hering, L. G. Hunsicker, D. B. Kaufman, O. Korsgren, C. P. Larsen, X. Luo, A. Naji, J. Oberholzer, A. M. Posselt, C. Ricordi, P. A. Senior, A. M. J. Shapiro, P. G. Stock, N. A. Turgeon, *Am. J. Transplant.* **2021**, *21*, 1477.
- [7] K. Verhoeff, B. A. Marfil-Garza, A. M. J. Shapiro, *Curr. Opin. Organ Transplant.* **2021**, *26*, 397.
- [8] S. Abadpour, C. C. Wang, E. M. Niemi, H. Scholz, *Curr. Transplant. Rep.* **2021**, *8*, 205.
- [9] P. Soon-Shiong, R. E. Heintz, N. Merideth, Q. X. Yao, Z. Yao, T. Zheng, M. Murphy, M. K. Moloney, M. Schmehl, M. Harris, R. Mendez, R. Mendez, P. A. Sandford, *Lancet* **1994**, *343*, 950.
- [10] R. Calafiore, G. Basta, G. Luca, A. Lemmi, M. P. Montanucci, G. Calabrese, L. Racanicchi, F. Mancuso, P. Brunetti, *Diabetes Care* **2006**, *29*, 137.
- [11] G. Basta, P. Montanucci, G. Luca, C. Boselli, G. Noya, B. Barbaro, M. Qi, K. P. Kinzer, J. Oberholzer, R. Calafiore, *Diabetes Care* **2011**, *34*, 2406.
- [12] S. Matsumoto, A. Abalovich, C. Wechsler, S. Wynyard, R. B. Elliott, *EBioMedicine* **2016**, *12*, 255.
- [13] S. Chen, J. Luo, L. Shen, X. Liu, W. Wang, J. Xu, Y. Ren, Y. Ye, G. Shi, F. Cheng, L. Cheng, X. Su, L. Dai, M. Gou, H. Deng, *ACS Appl. Mater. Interfaces* **2022**, *14*, 23139.
- [14] A. R. Mridha, T. R. Dargaville, P. D. Dalton, L. Carroll, M. B. Morris, V. Vaithilingam, B. E. Tuch, *Tissue Eng., Part A* **2022**, *28*, 212.
- [15] Y. N. Lee, H.-J. Yi, Y. H. Kim, S. Lee, J. Oh, T. Okano, *Cells* **2020**, *9*, 1999.
- [16] P. Apelgren, M. Amoroso, K. Säljö, M. Montelius, A. Lindahl, L. S. Orrhult, P. Gatenholm, L. Kölby, *Biomaterials* **2021**, *276*, 121002.
- [17] M. Bordon, E. Karabulut, V. Kuzmenko, V. Fantini, O. Pansarasa, C. Cereda, P. Gatenholm, *Cells* **2020**, *9*, 682.
- [18] P. Apelgren, E. Karabulut, M. Amoroso, A. Mantas, H. Martínez Ávila, L. Kölby, T. Kondo, G. Toriz, P. Gatenholm, *ACS Biomater. Sci. Eng.* **2019**, *5*, 2482.
- [19] D. M. Pedrotty, V. Kuzmenko, E. Karabulut, A. M. Sugrue, C. Livia, V. R. Vaidya, C. J. Mcleod, S. J. Asirvatham, P. Gatenholm, S. Kapa, *Circ.: Arrhythmia Electrophysiol.* **2019**, *12*, e006920.
- [20] P. Apelgren, M. Amoroso, A. Lindahl, C. Brantsing, N. Rotter, P. Gatenholm, L. Kölby, *PLoS One* **2017**, *12*, e0189428.
- [21] S. Jeon, J.-H. Heo, M. K. Kim, W. Jeong, H.-W. Kang, *Adv. Funct. Mater.* **2022**, *30*, 2005324.
- [22] Y. Xiang, K. Miller, J. Guan, W. Kiratitanaporn, M. Tang, S. Chen, *Arch. Toxicol.* **2022**, *96*, 691.
- [23] S. Khalil, W. Sun, *J. Biomech. Eng.* **2009**, *131*, 111002.
- [24] J.-S. Lee, J. M. Hong, J. W. Jung, J.-H. Shim, J.-H. Oh, D.-W. Cho, *Biofabrication* **2014**, *6*, 024103.
- [25] G. Helenius, H. Bäckdahl, A. Bodin, U. Nannmark, P. Gatenholm, B. Risberg, *J. Biomed. Mater. Res., Part A* **2006**, *76A*, 431.
- [26] K. Missoum, M. N. Belgacem, J. Bras, *Materials* **2013**, *6*, 1745.
- [27] K. Markstedt, A. Mantas, I. Tournier, H. Martínez Ávila, D. Hägg, P. Gatenholm, *Biomacromolecules* **2015**, *16*, 1489.
- [28] P. Apelgren, M. Amoroso, K. Säljö, A. Lindahl, C. Brantsing, L. S. Orrhult, P. Gatenholm, L. Kölby, *Plast. Reconstr. Surg. Glob. Open* **2018**, *6*, e1930.
- [29] K. Markstedt, A. Mantas, I. Tournier, H. M. Ávila, D. Hägg, P. Gatenholm, *Biomacromolecules* **2015**, *16*, 1489.
- [30] H. M. Ávila, S. Schwarz, N. Rotter, P. Gatenholm, *Tissue Eng., Part A* **2015**, *21*, S373.
- [31] J. Kim, I. K. Shim, D. G. Hwang, Y. N. Lee, M. Kim, H. Kim, S.-W. Kim, S. Lee, S. C. Kim, D.-W. Cho, J. Jang, *J. Mater. Chem. B* **2019**, *7*, 4592.
- [32] S. Duin, K. Schütz, T. Ahlfeld, S. Lehmann, A. Lode, B. Ludwig, M. Gelinsky, *Adv. Healthcare Mater.* **2019**, *8*, 1801631

- [33] G. Marchioli, L. Van Gurp, P. P. Van Krieken, D. Stamatialis, M. Engelse, C. A. Van Blitterswijk, M. B. J. Karperien, E. De Koning, J. Alblas, L. Moroni, A. A. Van Apeldoorn, *Biofabrication* **2015**, 7, 025009.
- [34] D. E. Per-Ola Carlsson, A. Sedigh, A. Rotem, B. Zimmerman, H. Grinberg, T. Goldman, U. Barkai, Y. Avni, G. T. Westermark, L. Carlsson, H. Ahlström, O. Eriksson, J. Olerud, O. Korsgren, *Am. J. Transplant.* **2018**, 18, 1735.
- [35] R. M. Spiers, S. E. Cross, H. L. Brown, P. A. Bateman, R. H. Vaughan, S. J. Hughes, P. R. V. Johnson, *Cell Transplant.* **2018**, 27, 1039.
- [36] A. Ebrahimi, M.-H. Jung, J. M. Dreyfuss, H. Pan, D. Sgroi, S. Bonner-Weir, G. C. Weir, *Islets* **2017**, 9, 19.
- [37] J. Kim, M. Kim, D. G. Hwang, I. K. Shim, S. C. Kim, J. Jang, *J. Vis. Exp.* **2019**, 154, e60434.
- [38] D. Wang, Y. Guo, J. Zhu, F. Liu, Y. Xue, Y. Huang, B. Zhu, D. Wu, H. Pan, T. Gong, Y. Lu, Y. Yang, Z. Wang, *Acta Biomater.* **2023**, 165, 86.
- [39] M. Buitinga, K. Janeczek Portalska, D.-J. Cornelissen, J. Plass, M. Hanegraaf, F. Carloti, E. De Koning, M. Engelse, C. Van Blitterswijk, M. Karperien, A. Van Apeldoorn, J. De Boer, *Tissue Eng., Part A* **2016**, 22, 375.
- [40] X. Liu, S.-S. D. Carter, M. J. Renes, J. Kim, D. M. Rojas-Canales, D. Penko, C. Angus, S. Beirne, C. J. Drogemuller, Z. Yue, P. T. Coates, G. G. Wallace, *Adv. Healthcare Mater.* **2019**, 8, e1801181.
- [41] G. A. Salg, E. Poisel, M. Neulinger-Munoz, J. Gerhardus, D. Cebulla, C. Bludszweit-Philipp, V. Vieira, F. Nickel, I. Herr, A. Blaesser, N. A. Giese, T. Hackert, H. G. Kenngott, *J. Tissue Eng.* **2022**, 13, 204173142210910.
- [42] R. Hass, C. Kasper, S. Böhm, R. Jacobs, *Cell Commun. Signaling* **2011**, 9, 12.
- [43] C. L. Rackham, P. K. Dhadda, P. C. Chagastelles, S. J. S. Simpson, A. A. Dattani, J. E. Bowe, P. M. Jones, A. J. F. King, *Cytotherapy* **2013**, 15, 449.
- [44] B. M. De Souza, A. P. Bouças, F. D. S. D. Oliveira, K. P. Reis, P. Ziegelmann, A. C. Bauer, D. Crispim, *Islets* **2017**, 9, 30.
- [45] X. Liang, Y. Ding, Y. Zhang, H.-F. Tse, Q. Lian, *Cell Transplant.* **2014**, 23, 1045.
- [46] H. Saijo, K. Suzuki, H. Yoshimoto, Y. Imamura, S. Yamashita, K. Tanaka, *Plast. Reconstr. Surg.* **2019**, 143, 1189e.
- [47] S. W. Schive, F. R., D. Josefsen, M. Katavic, S. Abadpour, H. P. Gullestad, G. Kvalheim, H. Scholz, *CellR4* **2018**, 6, e2519.
- [48] F. Veronesi, M. Maglio, M. Tschon, N. N. Aldini, M. Fini, *J. Biomed. Mater. Res., Part A* **2014**, 102, 2448.
- [49] S. W. Schive, M. R. Mirlashari, G. Hasvold, M. Wang, D. Josefsen, H. P. Gullestad, O. Korsgren, A. Foss, G. Kvalheim, H. Scholz, *Cell Med.* **2017**, 9, 103.
- [50] Y. Ohmura, M. Tanemura, N. Kawaguchi, T. Machida, T. Tanida, T. Deguchi, H. Wada, S. Kobayashi, S. Marubashi, H. Eguchi, Y. Takeda, N. Matsuura, T. Ito, H. Nagano, Y. Doki, M. Mori, *Transplantation* **2010**, 90, 1366.
- [51] T. M. Kono, E. K. Sims, D. R. Moss, W. Yamamoto, G. Ahn, J. Diamond, X. Tong, K. H. Day, P. R. Territo, H. Hanenberg, D. O. Traktuev, K. L. March, C. Evans-Molina, *Stem Cells* **2014**, 32, 1831.
- [52] A. Gamble, R. Pawlick, A. R. Pepper, A. Bruni, A. Adesida, P. A. Senior, G. S. Korbitt, A. M. J. Shapiro, *PLoS One* **2018**, 13, e0206449.
- [53] L. Cai, B. H. Johnstone, T. G. Cook, Z. Liang, D. Traktuev, K. Cornetta, D. A. Ingram, E. D. Rosen, K. L. March, *Stem Cells* **2007**, 25, 3234.
- [54] X. Wei, L. Zhao, J. Zhong, H. Gu, D. Feng, B. H. Johnstone, K. L. March, M. R. Farlow, Y. Du, *Neurosci. Lett.* **2009**, 462, 76.
- [55] A. S. Friberg, M. Ståhle, H. Brandhorst, O. Korsgren, D. Brandhorst, *Cell Transplant.* **2008**, 17, 1305.
- [56] A. S. Friberg, H. Brandhorst, P. Buchwald, M. Goto, C. Ricordi, D. Brandhorst, O. Korsgren, *Transplantation* **2011**, 91, 677.
- [57] A. Sahraoui, M. S. Winzell, T. Gorman, D. M. Smith, S. Skrtic, M. Hoeyem, S. Abadpour, L. Johansson, O. Korsgren, A. Foss, H. Scholz, *PLoS One* **2015**, 10, e0121204.
- [58] H. Brandhorst, D. Brandhorst, A. Abraham, S. Acreman, S. W. Schive, H. Scholz, P. R. V. Johnson, *Cell Transplant.* **2020**, 29, 096368972095233.
- [59] G. Boix-Lemonche, R. M. Nagymihaly, E. M. Niemi, N. Josifovska, S. Johansen, M. C. Moe, H. Scholz, G. Petrovski, *Macromol. Biosci.* **2023**, 23, e2200422.
- [60] P. Apelgren, M. Amoroso, K. Säljö, A. Lindahl, C. Brantsing, L. Stridh Orrhult, K. Markstedt, P. Gatenholm, L. Kölby, *J. Biomed. Mater. Res., Part B* **2021**, 109, 126.
- [61] J. N. Clark, A. Garbout, S. A. Ferreira, B. Javaheri, A. A. Pitsillides, S. M. Rankin, J. R. T. Jeffers, U. Hansen, *Osteoarthritis Cartilage* **2020**, 28, 102.
- [62] M. Kang, C. A. Day, A. K. Kenworthy, E. Dibenedetto, *Traffic* **2012**, 13, 1589.
- [63] D. M. Soumpasis, *Biophys. J.* **1983**, 41, 95.
- [64] C. Köhler, A. Gahm, T. Noma, A. Nakazawa, S. Orrenius, B. Zhivotovsky, *FEBS Lett.* **1999**, 447, 10.
- [65] M. Hårdstedt, S. Lindblom, A. Karlsson-Parra, B. Nilsson, O. Korsgren, *Cell Transplant.* **2016**, 25, 503.
- [66] R. L. Pawlick, J. Wink, A. R. Pepper, A. Bruni, N. Abualhassen, Y. Rafiei, B. Gala-Lopez, M. Bral, A. M. J. Shapiro, *Islets* **2016**, 8, 115.
- [67] A. Citro, E. Cantarelli, P. Maffi, R. Nano, R. Melzi, A. Mercalli, E. Dugnani, V. Sordi, P. Magistretti, L. Daffonchio, P. A. Ruffini, M. Allegretti, A. Secchi, E. Bonifacio, L. Piemonti, *J. Clin. Invest.* **2012**, 122, 3647.
- [68] J. J. Meier, B. A. Menge, T. G. K. Breuer, C. A. Müller, A. Tannapfel, W. Uhl, W. E. Schmidt, H. Schrader, *Diabetes* **2009**, 58, 1595.
- [69] A. R. Pepper, A. Bruni, A. M. J. Shapiro, *Curr. Opin. Organ Transplant.* **2018**, 23, 428.
- [70] L. De Moor, J. Smet, M. Plovyt, B. Bekaert, C. Vercruysse, M. Asadian, N. De Geyter, S. Van Vlierberghe, P. Dubruiel, H. Declercq, *Biofabrication* **2021**, 13, 045021.
- [71] P.-O. Carlsson, D. Espes, A. Sedigh, A. Rotem, B. Zimmerman, H. Grinberg, T. Goldman, U. Barkai, Y. Avni, G. T. Westermark, L. Carlsson, H. Ahlström, O. Eriksson, J. Olerud, O. Korsgren, *Am. J. Transplant.* **2018**, 18, 1735.
- [72] M. Bhattacharya, M. M. Malinen, P. Lauren, Y.-R. Lou, S. W. Kuisma, L. Kanninen, M. Lille, A. Corlu, C. Guguen-Guillouzo, O. Ikkala, A. Laukkanen, A. Urtti, M. Yliperttula, *J. Controlled Release* **2012**, 164, 291.
- [73] J. Göhl, K. Markstedt, A. Mark, K. Håkansson, P. Gatenholm, F. Edelvik, *Biofabrication* **2018**, 10, 034105.
- [74] D. Nguyen, D. A. Hägg, A. Forsman, J. Ekholm, P. Nimkingratana, C. Brantsing, T. Kalogeropoulos, S. Zaunz, S. Concaro, M. Brittberg, A. Lindahl, P. Gatenholm, A. Enejder, S. Simonsson, *Sci. Rep.* **2017**, 7, 658.
- [75] M. Amoroso, P. A., K. Säljö, M. Montelius, L. Orrhult, M. Engström, P. Gatenholm, L. Kölby, *Bioprinting* **2021**, 23, e00162.
- [76] M. Wang, M. Crager, S. Pugazhenthir, *Exp. Diabetes Res.* **2012**, 2012, 647914.
- [77] J. T. Daoud, M. S. Petropavlovskaya, J. M. Patapas, C. E. Degrandpré, R. W. DiRaddo, M. T. Lawrence-Rosenberg, *Biomaterials* **2011**, 32, 1536.
- [78] M. Hannula, A.-M. Haaparanta, I. Tamminen, A. Aula, M. Kellomaki, J. Hyttinen, *Annu. Int. Conf. IEEE Eng. Med. Biol. Soc.* **2015**, 2015, 5626.
- [79] A. Citro, H. C. Ott, *Curr. Diabetes Rep.* **2018**, 18, 122.
- [80] R. Wang, L. Rosenberg, *J. Endocrinol.* **1999**, 163, 181.
- [81] S. Abdelli, J. Ansire, R. Roduit, T. Borsello, I. Matsumoto, T. Sawada, N. Allaman-Pillet, H. Henry, J. S. Beckmann, B. J. Hering, C. Bonny, *Diabetes* **2004**, 53, 2815.
- [82] P. D. Campbell, A. Weinberg, J. Chee, L. Mariana, R. Ayala, W. J. Hawthorne, P. J. O'connell, T. Loudovaris, M. J. Cowley, T. W. Kay, S. T. Grey, H. E. Thomas, *Cell Transplant.* **2012**, 21, 49.

- [83] W. Y. Chung, C. A. Pollard, R. Kumar, C. J. Drogemuller, B. Naziruddin, C. Stover, E. Issa, J. Isherwood, J. Cooke, M. F. Levy, P. T. H. Coates, G. Garcea, A. R. Dennison, *Ann. Transl. Med.* **2021**, 9, 98.
- [84] R. Melzi, A. Mercalli, V. Sordi, E. Cantarelli, R. Nano, P. Maffi, G. Sitia, L. G. Guidotti, A. Secchi, E. Bonifacio, L. Piemonti, *Cell Transplant.* **2010**, 19, 1031.
- [85] M. J. Cowley, A. Weinberg, N. W. Zammit, S. N. Walters, W. J. Hawthorne, T. Loudovaris, H. Thomas, T. Kay, J. E. Gunton, S. I. Alexander, W. Kaplan, J. Chapman, P. J. O'connell, S. T. Grey, *Cell Transplant.* **2012**, 21, 2063.
- [86] A. Trzyna, A. Banas-Zabczyk, *Biomolecules* **2021**, 11, 878.
- [87] C. Giannasi, S. Niada, C. Magagnotti, E. Ragni, A. Andolfo, A. T. Brini, *Stem Cell Res. Ther.* **2020**, 11, 521.
- [88] L. Xue, H. P. Greisler, *Surgery* **2002**, 132, 259.
- [89] D. XiaoZhen, C. ShaoXi, Y. QunFang, J. JiaHuan, Y. XiaoQing, X. Xin, J. QiFeng, W. A. Chih-Lueh, T. Yi, *Chin. Sci. Bull.* **2011**, 56, 3301.
- [90] K. Säljö, P. Apelgren, L. Stridh Orrhult, S. Li, M. Amoroso, P. Gatenholm, L. Kölby, *Adipocyte* **2022**, 11, 34.
- [91] A. Scuteri, E. Donzelli, V. Rodriguez-Menendez, M. Ravasi, M. Monfrini, B. Bonandrini, M. Figliuzzi, A. Remuzzi, G. Tredici, *PLoS One* **2014**, 9, e84309.
- [92] B. M. de Souza, M. Rodrigues, F. S. de Oliveira, L. P. A. da Silva, A. P. Bouças, C. P. Portinho, B. P. Dos Santos, M. Camassola, D. Rocha, S. Lysakowski, J. Martini, C. B. Leitão, N. B. Nardi, A. C. Bauer, D. Crispim, *Mol. Cell. Endocrinol.* **2020**, 505, 110729.
- [93] J. Thévenet, V. Gmyr, N. Delalleau, F. Pattou, J. Kerr-Conte, *Lab. Anim.* **2021**, 55, 408.
- [94] S. Muratore, D. A. Thompson, M. Bellin, B. Bland, L. K. Berry, J. Wilhelm, T. B. Dunn, S. Chinnakotla, T. Pruett, G. Beilman, *J. Am. Coll. Surg.* **2016**, 223, S77.
- [95] M. Buitinga, R. Truckenmüller, M. A. Engelse, L. Moroni, H. W. M. Ten Hoopen, C. A. Van Blitterswijk, E. J. De Koning, A. A. Van Apeldoorn, M. Karperien, *PLoS One* **2013**, 8, e64772.
- [96] K. Verhoeff, B. A. Marfil-Garza, G. Sandha, D. Cooper, K. Dajani, D. L. Bigam, B. Anderson, T. Kin, A. Lam, D. O'gorman, P. A. Senior, C. Ricordi, A. M. J. Shapiro, *Transplantation* **2022**, 106, 2224.
- [97] K. Suzuki, S. Bonner-Weir, J. Hollister, G. C. Weir, *Cell Transplant.* **1996**, 5, 613.
- [98] E. Cantarelli, A. Citro, S. Marzorati, R. Melzi, M. Scavini, L. Piemonti, *Islets* **2013**, 5, 79.
- [99] H.-I. Kim, J. E. Yu, C.-G. Park, S.-J. Kim, *J. Korean Med. Sci.* **2010**, 25, 203.
- [100] P. de Vos, D. Vegter, B. J. de Haan, J. H. Strubbe, J. E. Bruggink, R. van Schilfgaarde, *Diabetes* **1996**, 45, 1102.
- [101] L. Zhang, K. Li, X. Liu, D. Li, C. Luo, B. Fu, S. Cui, F. Zhu, R. C. Zhao, X. Chen, *Stem Cells Dev.* **2013**, 22, 3074.